

SGC-AAK1-1: A Chemical Probe Targeting AAK1 and BMP2K

Carrow Wells,^{†,‡} Rafael M. Couñago,^{§,||} Juanita C. Limas,[#] Tuanny L. Almeida,^{§,||} Jeanette Gowen Cook,[⊥] David H. Drewry,^{†,‡} Jonathan M. Elkins,^{§,∇} Opher Gileadi,^{§,∇} Nirav R. Kapadia,^{†,‡} Alvaro Lorente-Macias,[○] Julie E. Pickett,^{†,‡} Alexander Riemen,[□] Roberta R. Ruela-de-Sousa,^{§,||} Timothy M. Willson,^{†,‡} Cunyu Zhang,[●] William J. Zuercher,^{†,‡,◆} Reena Zutshi,[□] and Alison D. Axtman^{*,†,‡}

[†]Structural Genomics Consortium (SGC), UNC Eshelman School of Pharmacy, University of North Carolina at Chapel Hill (UNC-CH), Chapel Hill, North Carolina 27599, United States

[‡]Division of Chemical Biology and Medicinal Chemistry, UNC Eshelman School of Pharmacy, UNC-CH, Chapel Hill, North Carolina 27599, United States

[§]SGC, Departamento de Genética e Evolução, Instituto de Biologia, Universidade Estadual de Campinas (UNICAMP), Campinas, SP 13083-886, Brazil

^{||}Centro de Química Medicinal, Centro de Biologia Molecular e Engenharia Genética, UNICAMP, Campinas, SP 13083-875, Brazil

[#]Department of Pharmacology, UNC-CH, Chapel Hill, North Carolina 27599, United States

[⊥]Department of Biochemistry and Biophysics, UNC-CH, Chapel Hill, North Carolina 27599, United States

[∇]SGC, Nuffield Department of Clinical Medicine, University of Oxford, Old Road Campus Research Building, Oxford, OX3 7DQ, U.K.

[○]Departamento de Química Farmacéutica y Orgánica, University of Granada, Granada, 18071, Spain

[◆]Lineberger Comprehensive Cancer Center (LCCC), UNC-CH, Chapel Hill, North Carolina 27599, United States

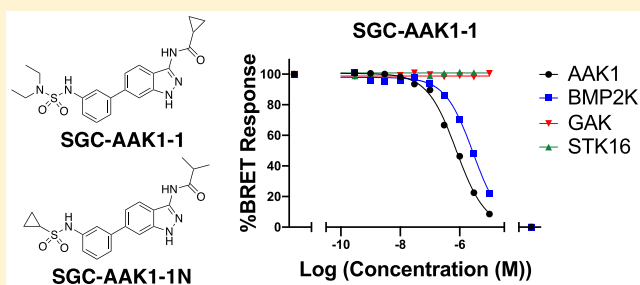
[□]Lucoome Biotechnologies, LLC, Tucson, Arizona 85719, United States

[●]Platform Technology Sciences, GlaxoSmithKline, Collegeville, Pennsylvania 19426, United States

S Supporting Information

ABSTRACT: Inhibitors based on a 3-acylaminoindazole scaffold were synthesized to yield potent dual AAK1/BMP2K inhibitors. Optimization furnished a small molecule chemical probe (SGC-AAK1-1, **25**) that is potent and selective for AAK1/BMP2K over other NAK family members, demonstrates narrow activity in a kinome-wide screen, and is functionally active in cells. This inhibitor represents one of the best available small molecule tools to study the functions of AAK1 and BMP2K.

KEYWORDS: AAK1, BMP2K, acylaminoindazole, NAK family, endocytosis, protein kinase



Human protein Ser/Thr kinases Adaptor protein 2-Associated Kinase 1 (AAK1) and BMP-2-Inducible Kinase (BMP2K/BIKE) play critical roles in mediating endocytosis and other key signaling pathways. Both are broadly expressed members of the NAK family of human kinases, which also includes Cyclin G-Associated Kinase (GAK) and Myristoylated and Palmitoylated Serine/Threonine Kinase 1 (MPSK1/STK16). The family shares little homology outside of their kinase domains (KDs).¹ AAK1 and BMP2K are the most closely related, with overall sequence identity of 50% and KD sequence identity of 74%.² A key function of AAK1 is regulation of receptor-mediated endocytosis via binding directly to clathrin and phosphorylating the medium subunit of AP2 (adaptor protein 2), which

stimulates binding to cargo proteins.³ AAK1 also modulates the Notch pathway, partially through its phosphorylation of Numb.^{4,5} BMP2K plays a role in osteoblast differentiation, is a clathrin-coated vesicle-associated protein, and, like AAK1, also associates with Numb.^{6,7}

Due to their many functions, AAK1 and BMP2K have been implicated as potential drug targets for diverse conditions. AAK1 has been linked to diseases affecting the brain such as

Special Issue: Women in Medicinal Chemistry

Received: August 29, 2019

Accepted: October 23, 2019

Published: October 23, 2019

schizophrenia, Parkinson's disease, and amyotrophic lateral sclerosis as well as implicated as a potential antiviral target for treatment of hepatitis C.^{8,9} BMP2K has been associated with myopia and evaluated as a potential treatment for HIV.^{10,11} Figure S1 shows the current inhibitor landscape and how their pharmacophores bind to AAK1/BMP2K. Patented AAK1 inhibitors were recently reviewed.¹²

X-ray crystal structures for the KDs of all NAK family members have been solved and reported.^{2,13} Published and novel high-resolution crystal structures of AAK1 and BMP2K reveal target-specific structural features that enabled our design of specific chemical probes and allowed further interrogation of the roles that these kinases play.² Screening a library of kinase inhibitors (Published Kinase Inhibitor Set, PKIS) via differential scanning fluorimetry (DSF) revealed a chemical starting point showing strong AAK1 binding.¹⁴ Structure–activity relationships (SAR) were initially established by examining the 3-acylaminoindazole analogs profiled within PKIS (Figures 1 and S2). Next, more than 200 analogs were prepared via the

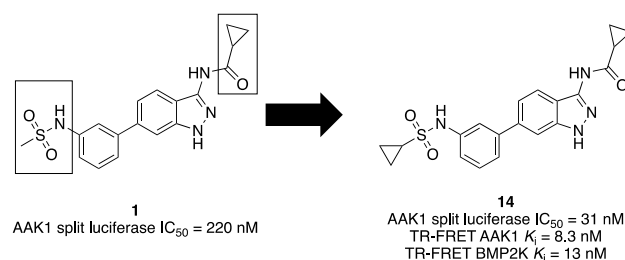


Figure 1. Structures of PKIS hit (1) and key analog 14 with parts of the molecule modified during SAR exploration.

route shown in Scheme S1. A summary of key analogs prepared to arrive at 14 is included in Table 1. Compounds were profiled using the AAK1 split luciferase assay developed by Lucoame.¹⁵ Potent inhibition of BMP2K was not observed in this assay format.

The effects of aryl substitution on the distal aryl ring were explored, including 3- and 4-position substituents of variable

Table 1. SAR of 3-Acylaminoindazole Aryl Ring

Compd	R	AAK1 IC_{50} (nM) ²²
1	3-NHSO ₂ Me	220
2	4-NHSO ₂ Me	1200
3	3-CONH ₂	3800
4	4-CONH ₂	910
5	3-NHAc	1100
6	3-CO ₂ H	18000
7	4-CO ₂ H	2800
8	3-OH	350
9	4-OH	280
10	3-NH ₂	800
11	3-N(CH ₃)SO ₂ Me	120
12	3-CH ₂ NHSO ₂ Me	71
13	3-NHSO ₂ (isopropyl)	54
14	3-NHSO ₂ (cyclopropyl)	31

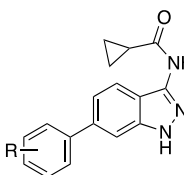
size, electronics, and hydrogen-bonding capacity (Table 1). A sulfonamide was found to be optimal for AAK1 inhibition but only when appended at the 3-position of the aryl ring (1 versus 2). Sulfonamides with small saturated rings (<6 atoms) and short alkyl chains or alkyl amines were the most potent (1, 11, 13, 14). This part of the binding pocket was not tolerant to incorporation of large groups. 3,5-Disubstitution and 3,6-disubstitution were disfavored, supporting a small binding pocket for this aryl ring that is sensitive to even minor changes, such as incorporation of a fluorine in place of a hydrogen (data not shown). Finally, activity of 1 and 8 suggests the presence of a hydrogen-bonding network within the ATP-binding pocket that can be accessed by 3-position groups capable of donating a hydrogen. Interestingly, methylation of the aryl 3-nitrogen (11) or insertion of a methylene spacer between the sulfonamide and aryl ring (12) increased potency for AAK1. These results motivated design of a range of sulfonamides to further explore the SAR of this part of the molecule.

The portion of the ATP-binding pocket accessed by the 3-position of the indazole was explored through substitution with a variety of groups (Table 2). Compounds in Table 2 were prepared using the route in Scheme S1, but the step order was reversed. The indazole 3-position substituent appears to form a polar interaction with the kinase hinge region and is sensitive to structural modifications. The alkyl group was varied from cyclopropyl to methyl, isopropyl, cyclobutyl, phenyl, and

Table 2. SAR of 3-Acylaminoindazole Carboxamide

Compd	R	AAK1 IC_{50} (nM) ²²
14		31
15		3500
16		18000
17		370
18		560
19		2200
20		>50000
21		>50000
22		7700

Table 3. NAK Family Binding-Displacement Assay Selectivity Analysis



Cmpd	R	AAK1 K_i (nM) ²³	BMP2K K_i (nM) ²³	GAK K_i (nM) ²³	STK16 K_i (nM) ²³
14	3-NHSO ₂ (cyclopropyl)	8.3	13	1600	330
23	3-NHSO ₂ N(CH ₃) ₂	10	19	2600	350
24	3-NHSO ₂ CH ₂ (cyclopropyl)	6.3	17	870	91

cyclopropylmethyl to explore the steric bulk tolerated by the pocket. Alternatively, a urea or sulfonamide was incorporated in place of the acylated amine (**20**, **21**, **22**) but resulted in loss of AAK1 affinity. The cyclopropanecarboxamide was found to be optimal (**14**). Minor changes, such as ring opening of the cyclopropane (**16**) or expansion to a cyclobutane (**17**), were found to result in loss of AAK1 affinity.

Based on the initial SAR, two additional 3-acylaminoindazoles (**23** and **24**) were prepared (Table 3) incorporating the aryl 3-cyclopropanecarboxamide that was found to yield potent inhibitors of AAK1. The analogs were designed to probe whether an alkyl amine or longer chain hydrocarbon could be tolerated at the indazole 3-position. Like lead compound **14**, these analogs demonstrated promising inhibition of AAK1 in the split luciferase assay (93%I and 94%I of AAK1 at 1 μ M for **23** and **24**, respectively). TR-FRET binding-displacement assays were employed to further interrogate the biochemical selectivity of these promising 3-aminoacylindazoles across the NAK family (Table 3).²¹ Compounds **23** and **24** were found to be dual AAK1/BMP2K inhibitors with more than 5-fold and 50-fold selectivity over STK16 and GAK, respectively.

To understand the selectivity of **23** and **24** across NAK family kinases, cocrystal structures were solved with the BMP2K KD (Figure 2, Table S1). Attempts to obtain cocrystals of acylaminoindazoles bound to the AAK1 KD were not successful. The BMP2K cocrystal structures were solved to \sim 2.4 Å resolution and showed that the core indazole formed the critical interaction with the hinge region of the KD.

Given the high structural and sequence conservation between the ATP-binding sites of the BMP2K and AAK1 KDs (Figures 2 and S3), it is likely that both kinases bind to the indazole inhibitors using common interactions. Thus it is unlikely, using this chemotype, that we can design inhibitors that target only AAK1 or BMP2K. The pendant aryl ring is accommodated by the hydrophobic region adjacent to the gatekeeper residue (residue Met130/126, BMP2K/AAK1 numbering) within the kinase ATP-binding site. These cocrystal structures suggest that large groups attached to the 4-position of the aryl ring (**2** and **4**) are likely not tolerated due to steric hindrance. Smaller groups at the 3- and 4-positions that can act as hydrogen-bond donors (**8** and **9**) can make favorable interactions with the DFG motif aspartate residue (Asp198/194), whereas small acidic groups at these positions (**6** and **7**) are not favored due to charge repulsion. The structures also reveal that a sulfonamide at the 3-position can form hydrogen-bonds with multiple polar residues within or adjacent to the protein ATP-binding pocket (Gln137/133, Asn185/181, and Asp198/194). Groups attached to this sulfonamide are accommodated by a small cavity within the protein P-loop. When considering substituents attached to the

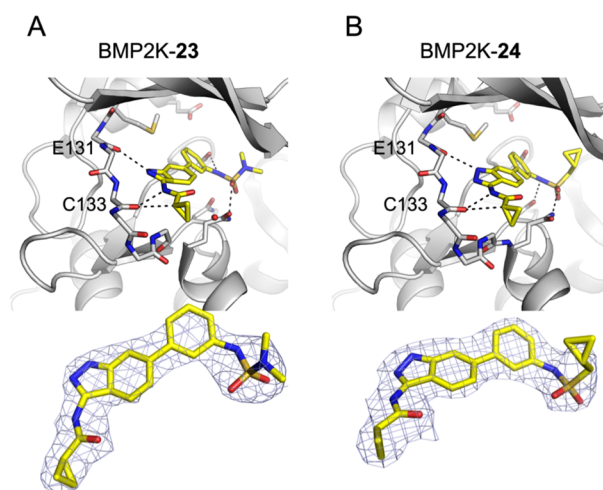
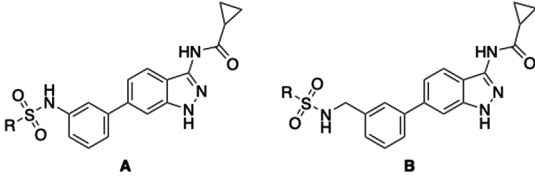


Figure 2. Cocrystal structures of **23** (A) and **24** (B) bound to the BMP2K-KD. Main-chain atoms for residues (131–137) within the BMP2K-KD hinge region, side-chain atoms for BMP2K-KD gatekeeper residue (Met130), and those taking part in polar interactions with the ligands are shown as sticks. Black dashed lines depict possible hydrogen-bonds between protein and ligand atoms. Red spheres denote the position of crystallographic water molecules. The 2Fo–Fc electron density maps (contoured at 1.0 σ) are shown below.

indazole ring, poor binding is observed for compounds bearing sulfonamide groups in place of an amide (**21** and **22**). This finding is due to steric clash and electronic effects caused by the proximity of the sulfonamide oxygen atoms to nearby protein side chains. Compound **20** is proposed to adopt a planar conformation that introduces a steric clash not observed with smaller groups and/or those that are not flat (**14** and **17**). Cocrystal structures also reveal that groups attached to the 3-position amide are solvent exposed, an observation that helps rationalize the moderate tolerance of AAK1 for larger and bulkier substituents at this position (**15**, **17**, and **19**).

Guided by these cocrystal structures, analogs were designed focusing on modifications to the sulfonamide portion of the molecule. Sulfonamides with pendant alkyl chains, alkyl amines, fluorinated alkyl chains, small hydrocarbon-based rings, and fluorinated aryl rings were synthesized. Table 4 includes some of our most promising analogs, the design of which was informed by more than 200 compounds prepared before them, some of which are included herein. Our years of effort on this scaffold enabled us to produce many highly potent compounds. Compounds built on Scaffold B were prepared via Scheme S1. Those built on Scaffold A were prepared using a slightly modified route (Scheme S2). Analogs **25–39** were evaluated for potency and selectivity across the

Table 4. *In Vitro* and Cellular SAR of 3-Acylaminoindazole Probe Candidates


Cmpd	Scaffold	R	AAK1 (nM)		BMP2K(nM)		GAK (nM)		STK16 (nM)		$S_{10}(1 \mu\text{M})^{26}$
			K_i^{23}	NB IC ₅₀ ²⁴	K_i^{23}	NB IC ₅₀ ²⁴	K_i^{23}	NB IC ₅₀ ²⁵	K_i^{23}	NB IC ₅₀ ²⁵	
14	A	cyclopropyl	8.3	641	13	1420	1600	>10000	330	>10000	0.005
25	A	N(CH ₂ CH ₃) ₂	9.1	770	17	2800	1700	>10000	270	>10000	0.02
26	A	N(CH ₂ CH ₃)(CH ₃)	8.2	375	20	1890	1700	>10000	310	>10000	0.017
27	A	CH ₂ CH(CH ₃) ₂	6.2	490	17	1490	1300	>10000	78	>10000	0.002
28	A	CH ₂ CH ₂ CH ₃	12	655	30	2180	1100	9250	110	>10000	0.01
29	A	4-F-benzyl	59	1020	120	2950	7000	9240	430	>10000	0.007
30	A	2-F-benzyl	22	528	51	1620	4600	>10000	470	>10000	0.022
31	A	3-F-benzyl	24	379	53	1190	4600	>10000	510	>10000	0.017
32	A	cyclobutyl	8.5	192	17	707	2900	>10000	240	>10000	0.007
33	B	CH ₂ CH ₂ CF ₃	32	2710	27	1890	510	>10000	180	>10000	0.022
34	B	N(CH ₂ CF ₃)(CH ₃)	44	3400	42	3030	780	>10000	290	>10000	
35	B	CH ₂ CF ₃	39	2350	33	1620	580	>10000	180	>10000	0.005
36	B	CH ₂ CH(CH ₃) ₂	30	1530	59	6550	3900	>10000	450	>10000	0.002
37	B	N(CH ₂ CH ₃) ₂	33	1470	74	3830	3200	>10000	220	>10000	
38	B	CH ₂ (cyclopropyl)	22	1260	37	2740	3200	>10000	150	>10000	0.01
39	B	N(CH ₂ CH ₃)(CH ₃)	20	1790	36	2960	360	>10000	86	>10000	

NAK family TR-FRET binding assays. Furthermore, cellular target engagement was determined via NanoBRET (NB) assays, where the respective kinases were fused to 19-kDa luciferase (NLuc) and transiently expressed in HEK293 cells, and then incubated with a cell-permeable fluorescent energy transfer probe (tracer).¹⁶ Using increasing concentrations of test compounds, dose-dependent displacement of the tracer was observed, allowing calculation of the IC₅₀ values in Table 4. These NB assays enabled measurement of potency and selectivity of the compounds across the NAK family in living cells (Figure S4).

All analogs (25–39) were found to be dual AAK1/BMP2K inhibitors. Insertion of the methylene spacer between the aryl ring and sulfonamide (Scaffold B) reduced potency for AAK1/BMP2K. Within the Scaffold B group of molecules, incorporation of an alkyl chain capped with fluorines (33, 34, and 35) increased the *in vitro* biochemical affinity for GAK, but not sufficiently to demonstrate GAK activity in cells (Table S3). In previous work, we had also observed that only low nanomolar inhibitors of GAK possessed cellular activity.¹⁷ Nearly all of the analogs were also devoid of activity in the STK16 NB assays. Several single-digit nanomolar biochemical inhibitors of AAK1 were prepared based upon Scaffold A that also demonstrated target engagement in cells with IC₅₀ values between 190–1020 nM. Incorporation of fluorinated aryl rings was tolerated by AAK1 and BMP2K but not by GAK or STK16 (29, 30, and 31).

3-Fluoroaryl analog (31) was one of the most potent compounds in the NB assays for AAK1 and BMP2K, while the 4-fluoro analog (29) was 3-fold less potent on both kinases. Compounds bearing small hydrocarbon chains and rings or alkyl amines on the sulfonamide proved to be the best dual AAK1/BMP2K inhibitors biochemically (14, 25, 26, 27, 28, and 32) and demonstrated at least 35-fold selectivity for BMP2K over GAK. The biochemical selectivity for BMP2K over STK16 was more variable (4–16-fold). When considering

the cell-based activity, 14, 26, 27, and 30–32 were the best performers in both AAK1 and BMP2K NB assays, while 25 and 28 exhibited a slight drop in potency when transitioning from the biochemical to cell-based assays. Confirmation of cell penetration and target engagement enables the facile translation of these compounds to *in vivo* studies. Furthermore, LipE was calculated for all compounds in Table 4 to estimate their quality as drug candidates (Figure S5).

All compounds from Table 4 built upon Scaffold A and a few representative compounds from Scaffold B (25–33, 35, 36, and 38) were evaluated for selectivity by KINOMEScan (DiscoverX) against 403 wildtype human protein kinases at 1 μM (Table 4).¹⁸ The compounds demonstrated remarkable selectivity for AAK1/BMP2K across the 403 human kinases. All proved to be narrow spectrum inhibitors of AAK1/BMP2K with >90% inhibition of only 1–9 kinases ($S_{10}(1 \mu\text{M}) = 0.005–0.022$, Figure S6).

To explore the phenotypic effect of AAK1/BMP2K inhibition, lead compound 14 and inactive analog 16 were tested in several cell lines. Surprisingly, we observed that 14 had cytostatic effects on cells after 24 h of continuous treatment. Further study in U2OS human osteosarcoma cells showed that 14 elicited cell cycle arrest in G2/M phase at 5–10 μM , which was not captured at the 5 μM dose (Figure S7). Although the molecular mechanism of the cell cycle arrest proved to be elusive, we employed U2OS cells as a screen to remove analogs that displayed this phenotype for consideration as chemical probes. A total of 12 analogs were screened for their effect on G2/M arrest (Figure 3). Nocodazole treatment was used as a positive control for a strong arrest in mitosis. Only analogs 27, 28, and 32 demonstrated the collateral G2 or M phase arrest at 5 μM , while the remaining analogs were devoid of this phenotype (Figures 3 and S8). Potent inhibition of AAK1/BMP2K by arrestors and nonarrestors alike indicated that G2 or M phase arrest was likely due to inhibition of an unidentified off-target kinase.

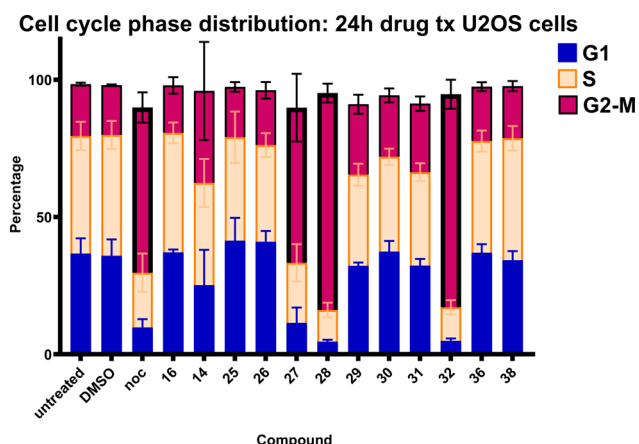


Figure 3. Cell cycle distributions. Cell cycle phases were determined by analytical flow cytometry of DNA content and DNA synthesis in U2OS cells after 24 h treatment with 5 μ M of the indicated compounds ($n = 3$).

Compounds **25** and **26** emerged as probe candidates based on their potency on AAK1 and BMP2K, kinome-wide selectivity, lack of a G2/M arresting phenotype, and LipE values. Following KINOMEScan of compounds **25** (SGC-AAK1-1) and **26**, the binding affinities (K_D) of all kinases inhibited >80% at 1 μ M plus AAK1 and a few kinases inhibited by structurally related analogs were determined (Table S4). Only three kinases were bound by **25** within 30-fold of the potency of **25** for AAK1: RIOK1 ($K_D = 72$), RIOK3 ($K_D = 290$), and PIP5K1C ($K_D = 260$).¹⁹ Compound **26** bound eight kinases within 30-fold of the potency of AAK1 (Table S4). Most compounds in Table 4 demonstrate potent affinity for RIOK1 and RIOK3 in the corresponding DiscoverX binding assays. Given that RIOK1 and RIOK3 are ATPases, an assay that has ATP present would be much more relevant but has not yet been developed.²⁰ In accordance with our previously described probe criteria,²¹ SGC-AAK1-1 (**25**) is a high quality dual AAK1/BMP2K chemical probe. Compound **16** (SGC-AAK1-1N) is the complementary negative control analog. The probe set has been made commercially available, making SGC-AAK1-1 the only AAK1-targeting chemical probe that is widely available alongside its negative control.

We have described the design, synthesis, and biological evaluation of a series of acylaminoindazoles as selective dual inhibitors of AAK1/BMP2K. Compound **25** emerged as our best probe candidate. X-ray cocrystal structures of selected acylaminoindazoles bound to BMP2K revealed key interactions within the ATP binding pocket that explain the high affinity of this series for AAK1 and BMP2K. The effect of **25** on WNT signaling was recently reported.¹⁹ Further investigations into effects of selective pharmacological inhibition of AAK1 are ongoing.

■ ASSOCIATED CONTENT

📄 Supporting Information

The Supporting Information is available free of charge on the ACS Publications website at DOI: [10.1021/acsmchemlett.9b00399](https://doi.org/10.1021/acsmchemlett.9b00399).

Protein crystallization conditions, NB and cell cycle assay details, experimental methods, and synthesis and characterization of compounds **25**, **26**, **27**, and **28** (PDF)

Accession Codes

PDB codes: compound **23**, 5I3O; compound **24**, 5I3R.

■ AUTHOR INFORMATION

Corresponding Author

*Tel: 919-962-5349. E-mail: alison.axtman@unc.edu.

ORCID

Carrow Wells: 0000-0003-4799-6792

David H. Drewry: 0000-0001-5973-5798

Nirav R. Kapadia: 0000-0002-2826-1689

Alvaro Lorente-Macias: 0000-0001-9510-714X

Julie E. Pickett: 0000-0002-9535-8528

Timothy M. Willson: 0000-0003-4181-8223

William J. Zuercher: 0000-0002-9836-0068

Alison D. Axtman: 0000-0003-4779-9932

Author Contributions

The manuscript was written through contributions of all authors. All authors have given approval to the final version of the manuscript.

Funding

SGC is a registered charity (number 1097737) that receives funds from AbbVie, Bayer Pharma AG, Boehringer Ingelheim, Canada Foundation for Innovation, Eshelman Institute for Innovation, Genome Canada, Innovative Medicines Initiative (EU/EFPIA) [ULTRA-DD 115766], Janssen, Merck KGaA Darmstadt Germany, MSD, Novartis Pharma AG, Ontario Ministry of Economic Development and Innovation, Pfizer, São Paulo Research Foundation-FAPESP [2013/50724-5, 2014/50897-0, 2016/17469-0], Takeda, and Wellcome [106169/ZZ14/Z]. This work was also supported by the Brazilian agency CNPq [465651/2014-3]. J.G.C. is supported by grants from the NIH/NIGMS (GM083024, and R25GM089569); J.C.L. is supported by an HHMI Gilliam Fellowship for Advanced Study (GT10886) and a T32 award (T32GM007040). The UNC Flow Cytometry Core Facility is supported in part by P30 CA016086 to the UNC LCCC. NC Biotech Center Institutional Support Grants 2017-IDG-1025 and 2018-IDG-1030 and NIH 1UM2AI30836-01 enabled this work. A.L.M. acknowledges support from the Spanish MEC (FPU 14/00818). D.H.D. and R.N. acknowledge 1R44TR001916 for support.

Notes

The authors declare no competing financial interest.

■ ACKNOWLEDGMENTS

R.M.C. thanks Diamond Light Source for access to beamline I03 (proposal number MX14664) that contributed to the results presented here. Constructs for NanoBRET measurements of AAK1, BMP2K, GAK, and STK16 were kindly provided by Promega. Dr. Ehrmann from the UNC Mass Spectrometry Core Laboratory provided HRMS support.

■ ABBREVIATIONS

AAK1, AP2-associated protein kinase 1; BMP2K/BIKE, BMP2-inducible kinase; STK16, serine/threonine kinase 16; GAK, cyclin-G-associated kinase; NAK, numb-associated kinase; AP2, adaptor protein 2; TR-FRET, time-resolved fluorescence resonance energy transfer; PKIS, published kinase inhibitor set; DSF, differential scanning fluorimetry; SAR, structure–activity relationships; HEK, human embryonic kidney; NB, NanoBRET; U2OS, U2 osteosarcoma; KD,

kinase domain; NLuc, nanoluciferase; tx, treatment; LipE, lipophilic efficiency

REFERENCES

- (1) Smythe, E.; Ayscough, K. R. The Ark1/Prk1 family of protein kinases. Regulators of endocytosis and the actin skeleton. *EMBO Rep.* **2003**, *4* (3), 246–51.
- (2) Sorrell, F. J.; Szklarz, M.; Abdul Azeez, K. R.; Elkins, J. M.; Knapp, S. Family-wide Structural Analysis of Human Numb-Associated Protein Kinases. *Structure* **2016**, *24* (3), 401–11.
- (3) Conner, S. D.; Schmid, S. L. Identification of an adaptor-associated kinase, AAK1, as a regulator of clathrin-mediated endocytosis. *J. Cell Biol.* **2002**, *156* (5), 921–9.
- (4) Gupta-Rossi, N.; Ortica, S.; Meas-Yedid, V.; Heuss, S.; Moretti, J.; Olivo-Marin, J. C.; Israel, A. The adaptor-associated kinase 1, AAK1, is a positive regulator of the Notch pathway. *J. Biol. Chem.* **2011**, *286* (21), 18720–30.
- (5) Sorensen, E. B.; Conner, S. D. AAK1 regulates Numb function at an early step in clathrin-mediated endocytosis. *Traffic* **2008**, *9* (10), 1791–800.
- (6) Borner, G. H.; Antrobus, R.; Hirst, J.; Bhumbra, G. S.; Kozik, P.; Jackson, L. P.; Sahlender, D. A.; Robinson, M. S. Multivariate proteomic profiling identifies novel accessory proteins of coated vesicles. *J. Cell Biol.* **2012**, *197* (1), 141–60.
- (7) Krieger, J. R.; Taylor, P.; Gajadhar, A. S.; Guha, A.; Moran, M. F.; McGlade, C. J. Identification and selected reaction monitoring (SRM) quantification of endocytosis factors associated with Numb. *Mol. Cell. Proteomics* **2013**, *12* (2), 499–514.
- (8) Neveu, G.; Barouch-Bentov, R.; Ziv-Av, A.; Gerber, D.; Jacob, Y.; Einav, S. Identification and targeting of an interaction between a tyrosine motif within hepatitis C virus core protein and AP2M1 essential for viral assembly. *PLoS Pathog.* **2012**, *8* (8), No. e1002845.
- (9) Shi, B.; Conner, S. D.; Liu, J. Dysfunction of endocytic kinase AAK1 in ALS. *Int. J. Mol. Sci.* **2014**, *15* (12), 22918–32.
- (10) Liu, H. P.; Lin, Y. J.; Lin, W. Y.; Wan, L.; Sheu, J. J.; Lin, H. J.; Tsai, Y.; Tsai, C. H.; Tsai, F. J. A novel genetic variant of BMP2K contributes to high myopia. *J. Clin. Lab. Anal.* **2009**, *23* (6), 362–7.
- (11) Zhou, H.; Xu, M.; Huang, Q.; Gates, A. T.; Zhang, X. D.; Castle, J. C.; Stec, E.; Ferrer, M.; Strulovici, B.; Hazuda, D. J.; Espeseth, A. S. Genome-scale RNAi screen for host factors required for HIV replication. *Cell Host Microbe* **2008**, *4* (5), 495–504.
- (12) Verdonck, S.; Pu, S.-Y.; Sorrell, F. J.; Elkins, J. M.; Froeyen, M.; Gao, L.-J.; Prugar, L. I.; Dorosky, D. E.; Brannan, J. M.; Barouch-Bentov, R.; Knapp, S.; Dye, J. M.; Herdewijn, P.; Einav, S.; De Jonghe, S. Synthesis and Structure–Activity Relationships of 3,5-Disubstituted-pyrrolo[2,3-b]pyridines as Inhibitors of Adaptor-Associated Kinase 1 with Antiviral Activity. *J. Med. Chem.* **2019**, *62* (12), 5810–5831.
- (13) Eswaran, J.; Bernad, A.; Ligos, J. M.; Guinea, B.; Debreczeni, J. E.; Sobott, F.; Parker, S. A.; Najmanovich, R.; Turk, B. E.; Knapp, S. Structure of the human protein kinase MPSK1 reveals an atypical activation loop architecture. *Structure* **2008**, *16* (1), 115–24.
- (14) Elkins, J. M.; Fedele, V.; Szklarz, M.; Abdul Azeez, K. R.; Salah, E.; Mikolajczyk, J.; Romanov, S.; Sepetov, N.; Huang, X. P.; Roth, B. L.; Al Haj Zen, A.; Fourches, D.; Muratov, E.; Tropsha, A.; Morris, J.; Teicher, B. A.; Kunkel, M.; Polley, E.; Lackey, K. E.; Atkinson, F. L.; Overington, J. P.; Bamborough, P.; Muller, S.; Price, D. J.; Willson, T. M.; Drewry, D. H.; Knapp, S.; Zuercher, W. J. Comprehensive characterization of the Published Kinase Inhibitor Set. *Nat. Biotechnol.* **2016**, *34* (1), 95–103.
- (15) Jester, B. W.; Cox, K. J.; Gaj, A.; Shomin, C. D.; Porter, J. R.; Ghosh, I. A coiled-coil enabled split-luciferase three-hybrid system: applied toward profiling inhibitors of protein kinases. *J. Am. Chem. Soc.* **2010**, *132* (33), 11727–35.
- (16) Vasta, J. D.; Corona, C. R.; Wilkinson, J.; Zimprich, C. A.; Hartnett, J. R.; Ingold, M. R.; Zimmerman, K.; Machleidt, T.; Kirkland, T. A.; Huwiler, K. G.; Ohana, R. F.; Slater, M.; Otto, P.; Cong, M.; Wells, C. I.; Berger, B. T.; Hanke, T.; Glas, C.; Ding, K.; Drewry, D. H.; Huber, K. V. M.; Willson, T. M.; Knapp, S.; Muller, S.; Meisenheimer, P. L.; Fan, F.; Wood, K. V.; Robers, M. B. Quantitative, Wide-Spectrum Kinase Profiling in Live Cells for Assessing the Effect of Cellular ATP on Target Engagement. *Cell Chem. Biol.* **2018**, *25* (2), 206–214.
- (17) Asquith, C. R. M.; Laitinen, T.; Bennett, J. M.; Godoi, P. H.; East, M. P.; Tizzard, G. J.; Graves, L. M.; Johnson, G. L.; Dornsife, R. E.; Wells, C. I.; Elkins, J. M.; Willson, T. M.; Zuercher, W. J. Identification and Optimization of 4-Anilinoquinolines as Inhibitors of Cyclin G Associated Kinase. *ChemMedChem* **2018**, *13* (1), 48–66.
- (18) Davis, M. I.; Hunt, J. P.; Herrgard, S.; Ciceri, P.; Wodicka, L. M.; Pallares, G.; Hocker, M.; Treiber, D. K.; Zarrinkar, P. P. Comprehensive analysis of kinase inhibitor selectivity. *Nat. Biotechnol.* **2011**, *29* (11), 1046–51.
- (19) Agajanian, M. J.; Walker, M. P.; Axtman, A. D.; Ruela-de-Sousa, R. R.; Serafin, D. S.; Rabinowitz, A. D.; Graham, D. M.; Ryan, M. B.; Tamir, T.; Nakamichi, Y.; Gammons, M. V.; Bennett, J. M.; Counago, R. M.; Drewry, D. H.; Elkins, J. M.; Gileadi, C.; Gildadi, O.; Godoi, P. H.; Kapadia, N.; Muller, S.; Santiago, A. S.; Sorrell, F. J.; Wells, C. I.; Fedorov, O.; Willson, T. M.; Zuercher, W. J.; Major, M. B. WNT activates the AAK1 kinase to promote clathrin-mediated endocytosis of LRP6 and establish a negative feedback loop. *Cell Rep.* **2019**, *26* (1), 79–83.
- (20) Weinberg, F.; Reischmann, N.; Fauth, L.; Taromi, S.; Mastroianni, J.; Köhler, M.; Halbach, S.; Becker, A. C.; Deng, N.; Schmitz, T.; Uhl, F. M.; Herbener, N.; Riedel, B.; Beier, F.; Swarbrick, A.; Lassmann, S.; Dengjel, J.; Zeiser, R.; Brummer, T. The Atypical Kinase R1OK1 Promotes Tumor Growth and Invasive Behavior. *EBioMedicine* **2017**, *20*, 79–97.
- (21) Asquith, C. R. M.; Berger, B.-T.; Wan, J.; Bennett, J. M.; Capuzzo, S. J.; Crona, D. J.; Drewry, D. H.; East, M. P.; Elkins, J. M.; Fedorov, O.; Godoi, P. H.; Hunter, D. M.; Knapp, S.; Müller, S.; Torrice, C. D.; Wells, C. I.; Earp, H. S.; Willson, T. M.; Zuercher, W. J. SGC-GAK-1: A Chemical Probe for Cyclin G Associated Kinase (GAK). *J. Med. Chem.* **2019**, *62* (5), 2830–2836.
- (22) Each test compound was screened in AAK1 split luciferase assay in duplicate ($n = 2$) against AAK1 in dose–response (8-pt curve).
- (23) Each test compound was screened in duplicate ($n = 2$) in TR-FRET binding-displacement assay in dose–response (16-pt curve). To allow comparison between different kinases, IC_{50} values (Table S2) were converted to K_i values using the Cheng–Prusoff equation and the concentration and K_D values for the tracer.
- (24) AAK1 and BMP2K NB cellular assays were performed in triplicate ($n = 3$) to provide IC_{50} values (11-pt curve).
- (25) STK16 and GAK NB cellular assays performed in singlicate ($n = 1$) based on demonstration of poor activity.
- (26) Calculation of S_{10} discussed in Figure S6.